In situ non-aqueous nucleation and growth of next generation rare-earth-free permanent magnets

Hyojung Yoon[a,b], Aoran Xu[a], George E. Sterbinsky[c], Dario A. Arena[c], Ziying Wang[a], Peter W. Stephens[d], Ying Shirley Meng[a,b*] and Kyler J. Carroll[a,e*]

[a] *Department of NanoEngineering, University of California San Diego, La Jolla, CA 92093, USA, E-mail: shmeng@ucsd.edu*
[b] *Materials Science and Engineering program, University of California San Diego, La Jolla, CA 92093, USA*
[c] *National Synchrotron Light Source, Brookhaven National Laboratory, Upton, NY 11973, USA*
[d] *Department of Physics and Astronomy, Stony Brook University, Stony Brook, NY 11794, USA*
[e] *Chemical Engineering, Massachusetts Institute of Technology, Cambridge, MA 01239, USA*

E-mail: shmeng@ucsd.edu, kcarroll@mit.edu

To whom correspondence should be addressed. E-mail: kcarroll@mit.edu, shmeng@ucsd.edu

1. Polyol Process of Cobalt Metal and Carbide

Table S1. Description of the conducted experiments.

Reaction	KOH (g)	CoCl2 (g)	$[Co^{2+}]/[OH^-]$
Cobalt Metal	0.2	0.6	0.69
Cobalt Carbide	0.8	0.6	0.17

2. High-resolution Powder X-ray Diffraction of Cobalt Metal and Carbide

High-resolution powder x-ray diffraction results of the Rietveld crystallographic analysis of cobalt carbide sample and their crystal structures are given in the Table S2 and Fig. S1.

Table S2. Crystallographic details of the sample Co carbide.

Phase	Co_2C
Space Group	*Pnnm* (#58)
Lattice Parameters (Å)	*a* = 4.371(1), *b* = 4.478(1), *c* = 2.881(1)
Mass Fraction	28(1)%
Atomic positions	Co: 4*g* 0.268(2), 0.346(1), 0
	C: 2*a* 0, 0, 0
Minimum bond length (Å): Co-C	1.89(1)
Co-Co	2.46(1)
Phase:	Co_3C
Space Group	*Pnma* (#62)
Lattice Parameters (Å)	*a* = 5.000(1), *b* = 6.739(2), *c* = 4.465(1)
Mass Fraction	72(1)%
Atomic positions	Co1: 8*d* 0.192(1), 0.063(1), 0.329(1)
	Co2: 4*c* 0.030(1), ¼, 0.836(1)
	C: 4*c* 0.960(1), ¼, 0.378(1)
Minimum bond length (Å): Co-C	1.73(2)
Co-Co	2.46(2)
Scherrer size parameter (restrained common to both phases)	220(10) Å
X-ray wavelength	0.69978(3) Å
R_{wp} [a]	5.06 %
R_{exp} [a]	1.87 %
GOF [a]	2.70

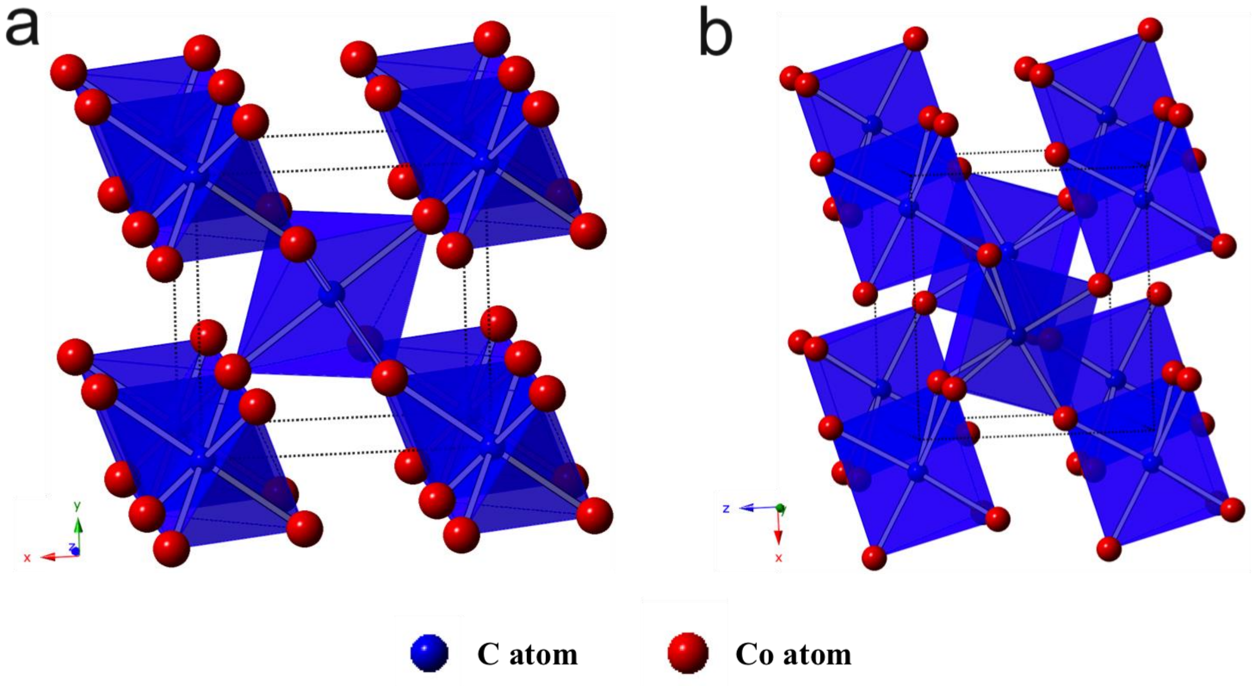

Figure S1. Crystal structures for Co_2C (a) and Co_3C (b).

The powder weighted *R*-factor is defined as

$$R_{\mathrm{wp}} = \sqrt{\frac{\sum_i w_i (y_i^{calc} - y_i^{obs})^2}{\sum_i w_i (y_i^{obs})^2}},$$

which has an expected value of

$$R_{\exp} = \sqrt{\frac{N}{\sum_i w_i (y_i^{obs})^2}}$$

if the Rietveld model is a perfect fit to the data, subject to statistical fluctuations. Here y_i^{calc} and y_i^{obs} are the calculated and observed intensities at the i^{th} point in the profile, normalized to monitor intensity. The weight w_i is $1/\sigma^2$ from the counting statistics, with the same normalization factor. *N* is the number of points in the measured profile, minus the number of refined parameters. GOF = R_{wp} / R_{exp}, is the square root of χ^2.

As shown in Fig. S2, the structure of metallic Co could not be satisfactorily fitted either as a combination of FCC and HCP lattices or as a random stacking of close-packed layers. These failures led us to study structures in which there was a degree of coherence between FCC and HCP regions which were several layers in extent.

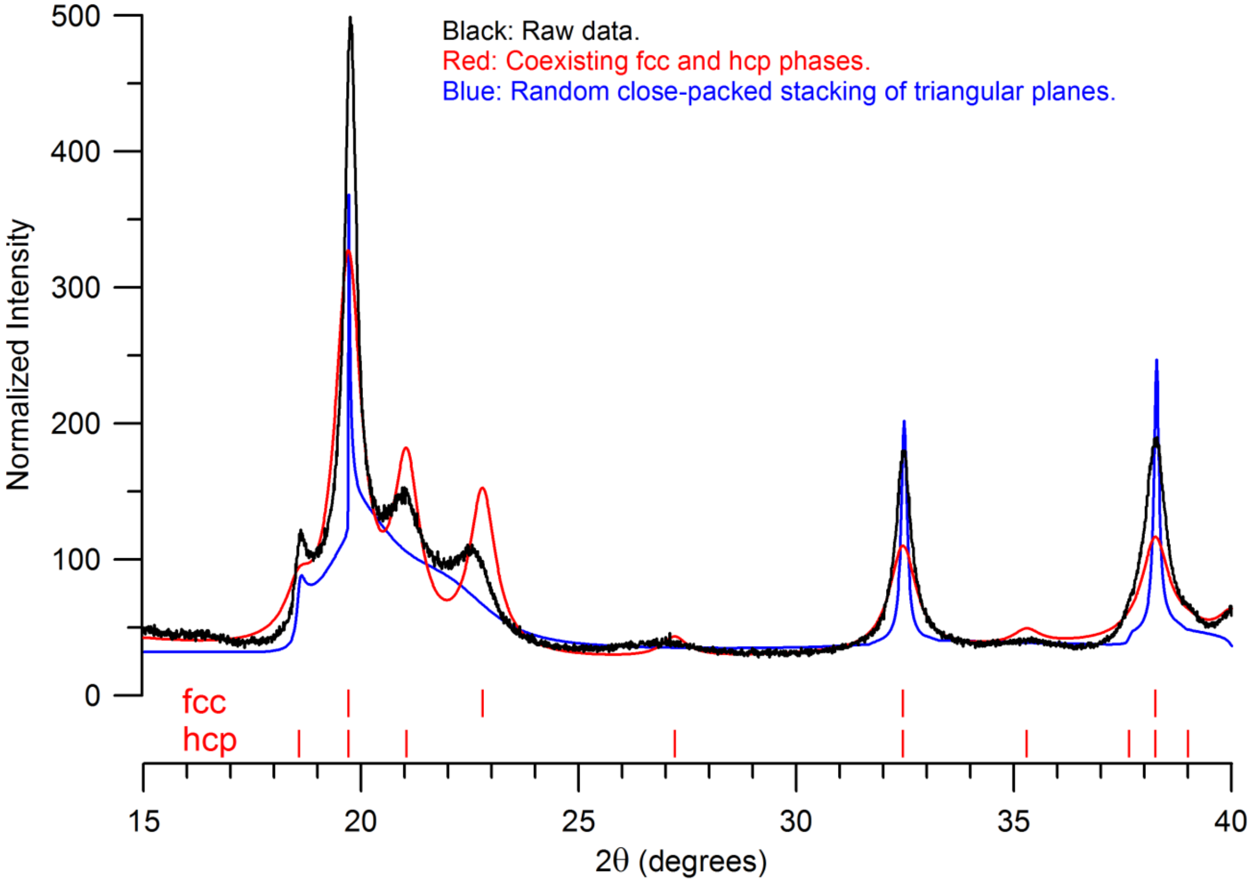

Figure S2. Powder diffraction data of a sample of heavily faulted metallic Co, compared to models of coexisting FCC and HCP phases (red) and a random close-packed stacking of triangular phases (blue).

3. Raman Spectra of Cobalt Metal and Carbide

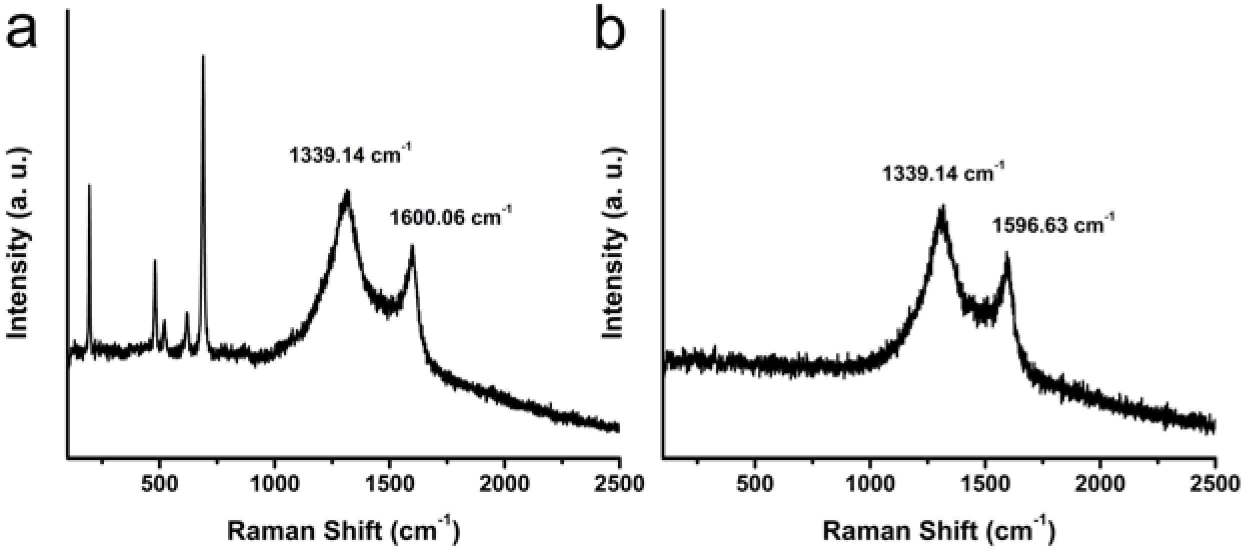

Figure S3. Raman spectra of the Co metal (a), and carbide (b) particles showing two types of D-G bands.

Micro-Raman spectroscopy is one of the most informative methods for investigation of the microstructure of carbon. It is well known that natural diamond has a single Raman peak at 1332 cm^{-1}, whereas crystalline graphite has a Raman peak referred to a the G peak around 1580 cm^{-1} originated from E_{2g} symmetry of bond-stretching vibrations of sp^2 carbon sites[1]. Nanocrystalline graphite and amorphous carbon have an additional peak referred to as the D peak at around 1355 cm^{-1} and originated from the A_{1g} breathing vibrations of the sixfold carbon rings. The D mode is forbidden in an ideal graphite structure, but appears when the disorder increases[2]. The width of the G and D peaks is due to the bond disorder of the sp^2 sites, while the D peak is only due to the sixfold carbon rings[3]. The spectra of the cobalt metal and carbide particles both show D-G band at around 1335 cm^{-1} and 1600 cm^{-1}. It has been reported that the position of the G peak moves to 1600 cm^{-1} when crystallized graphite change to nanocrystalline graphite[4]. Therefore, it can be confirmed that the G band positions of the cobalt metal and carbide are close to that of nanocrystalline graphite of nanometer-sized clusters.

Metal-metal and metal-ligand vibrations have frequencies below 750 cm^{-1}. This mode is the most sensitive to reveal the strength of metal-metal bonding. The symmetric and asymmetric stretching frequencies of metal lie in a range 150-650 cm^{-1} depending on the metal-metal bonding and the symmetric stretching mode strongly active in Raman spectra[5]. Moreover, the metal-related line intensity is enhanced in resonance Raman spectra because it excites the molecules in the red-end of their d-d transition[6]. The Raman peaks below 750 cm^{-1} are attributed to the Co-Co stretching mode, observed in Fig. S3a.

4. HR TEM and Lorentz micrographs

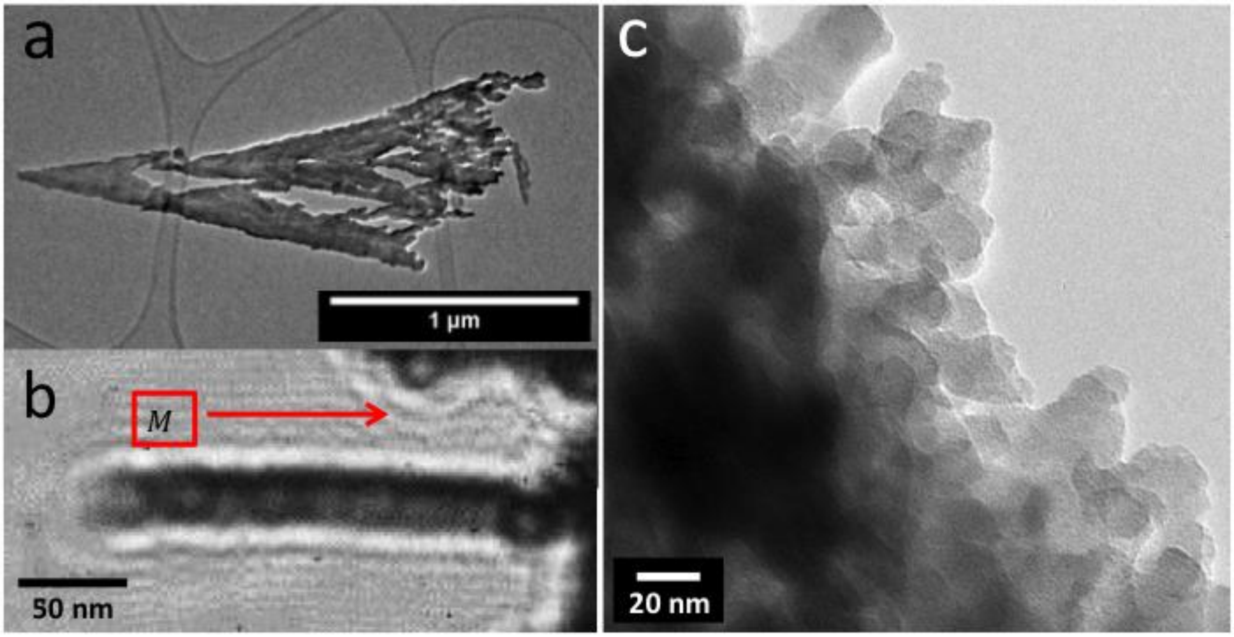

Figure S4. Lorentz micrographs of Co carbide particles.

Fig. S4 shows a series of Lorentz micrographs, observed in just-focused (a) and (c) and enlarged images under over-focused conditions. The defocused image (Fig. S4b) reveal speckled contrast, showing bright/dark meandering lines. From these images, the sizes of the speckled were evaluated to be ~30 nm or smaller. In large-grained materials, well-defined, multiple magnetic domains are observed within individual physical grains. Magnetic domain boundaries interior to nanometer-scaled grains are likely to be too energetic, so that either single magnetic domains are defined concurrently with the physical grains.

5. Quantitative kinetic study of the Co metal and carbide formation

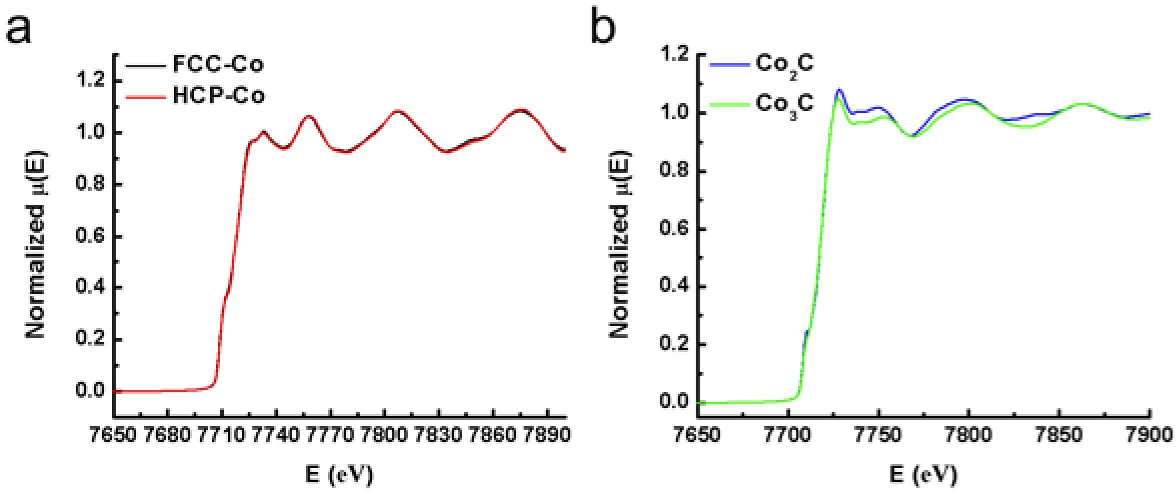

Figure S5. *Ex situ* Co K-edge XANES spectra for Co metal (a) and Co carbide (b) after running reactions.

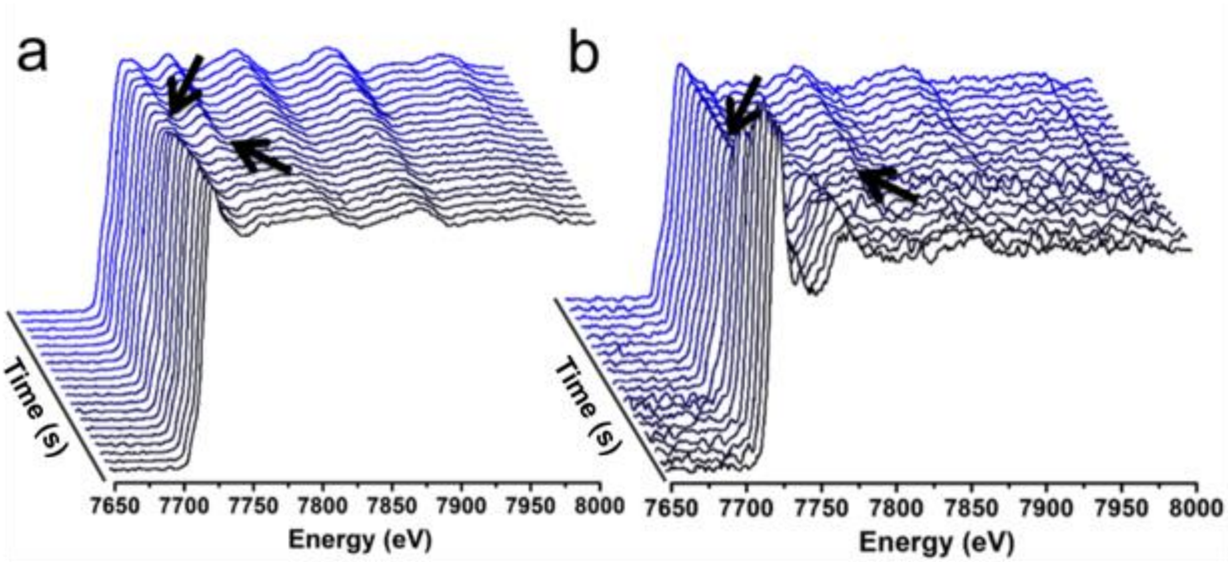

Figure S6. Time evolution as a function of the reduction time for Co K-edge XANES spectra for Co metal (a) and Co carbide (b).

The final products were directly obtained from each reaction and washed several times with ethanol to remove residue. After drying them, the two different final products were characterized by *ex situ* XAS spectra, taken in transmission mode. Fig. S5 shows the normalized XANES spectra: Co metal (a) and Co carbide (b). To derive nucleation and growth rate for the formation pathway, they are defined such that R_t, R_0, R_{3300}, and R_{3900} are the values of absorbance μ at reaction time of t, 0, 3300 and 3900 sec, respectively, where E is a value of the intrinsic energy related to the Co metal and carbide contribution as indicated by the arrow. For example, in the case of Co metal formation, the amount of unreacted Co^{2+} at the reaction time of 0 s, which is abbreviated as $[Co^{2+}_{precursor}]_0$, should be proportional to the difference (R_0-R_{3900}). Similarly, the amount of unreduced Co^{2+} at the reaction time of t s, which is abbreviated as $[Co^{2+}_{precursor}]_t$, should be proportional to the difference (R_t-R_{3900}). Therefore, the values of $[Co^{2+}_{precursor}]_t/[Co^{2+}_{precursor}]_0$ are regarded as those of $[(R_t-R_{3900})/(R_0-R_{3900})]$.

6. Modification of FW 2-step model

Finke and Watzky have proposed a two-step mechanism for the reduction of transition-metal salts; for example, a precursor complex of $[Bu_4N]_5Na_3[(1,5\text{-}COD\_Ir{\cdot}P_2W_{15}Nb_3O_{62}]$ under H_2 that consists of (a) slow, continuous nucleation, followed by (b) fast, autocatalytic surface growth[7]. (a) A→B (rate constant k_1) then (b) A + B → 2B (rate constant k_2), where A is a precursor complex and B is a surface atom of the nanoclusters. Hence, by following the concentration changes of these steps, we can follow the nanocluster formation reaction and its kinetics. We can obtain the kinetic information on the net reaction of steps (a) and (b), that is $-d[A]/dt = k_1[A] + k_2[A]([A]_0 - [A])$. The applicable rate equation is given as,

$$[A]_t = \frac{\frac{k_1}{k_2} + [A]_0}{1 + \frac{k_1}{k_2[A]_0} exp[(k_1 + k_2[A]_0)t]}$$

where k_1 is the rate constant for the first nucleation step and k_2 is the rate constant for the following autocatalytic growth step, respectively[8]. $[A]_t$ and $[A]_0$ are the concentration of nanocluster precursor A at a certain reaction time t and initial. The FW model needs to be converted to have the same mole fraction term (α) to compare fit results between the AE and FW model. By introducing $[A]_t = [A_0](1-\alpha)$ to the FW rate equation above the resulting equation in turn allows the AE and FW models to be directly compared.

$$\alpha = 1 - \frac{k_1 + k_2'}{k_2' + k_1 exp[(k_1 + k_2')t]}$$

7. Fitting results for Co-metal and carbide formation

Table S3. Fitting results based on the AE and FW equation for Co-metal and Co-carbide formation.

Reaction	Sample $[Co^{2+}]/[OH^-]$	AE model		FW model	
		k (s^{-1})	n	$k_{1,obs}$ (s^{-1})	$k_{2,obs}$ ($s^{-1}M^{-1}$)
Cobalt Metal	0.69	6.726×10^{-4} ± 0.4369 %	4	1.205×10^{-6} ± 6.0072 %	6.242×10^{-3} ± 0.4681 %
Cobalt Carbide	0.17	1.319×10^{-3} ± 0.4549 %	3	5.872×10^{-5} ± 8.0722 %	6.990×10^{-3} ± 2.1459 %

8. EXAFS Analysis results for Co metal and carbide formation

Fig. S7 and Table S4 provide results of the EXAFS fitting, including the raw and fitted χ(k) spectra. It also contains the raw and fitted Fourier transform magnitude spectra of the final reaction products, interpreted from the *ex situ* powder XAS spectra from Fig. S5. EXAFS data reduction and fitting were carried out using the Artemis and FEFF 9 programs to confirm the final phases. The k and R ranges were approximately 2 - 8 $Å^{-1}$ and 1.0 - 4.0 Å.

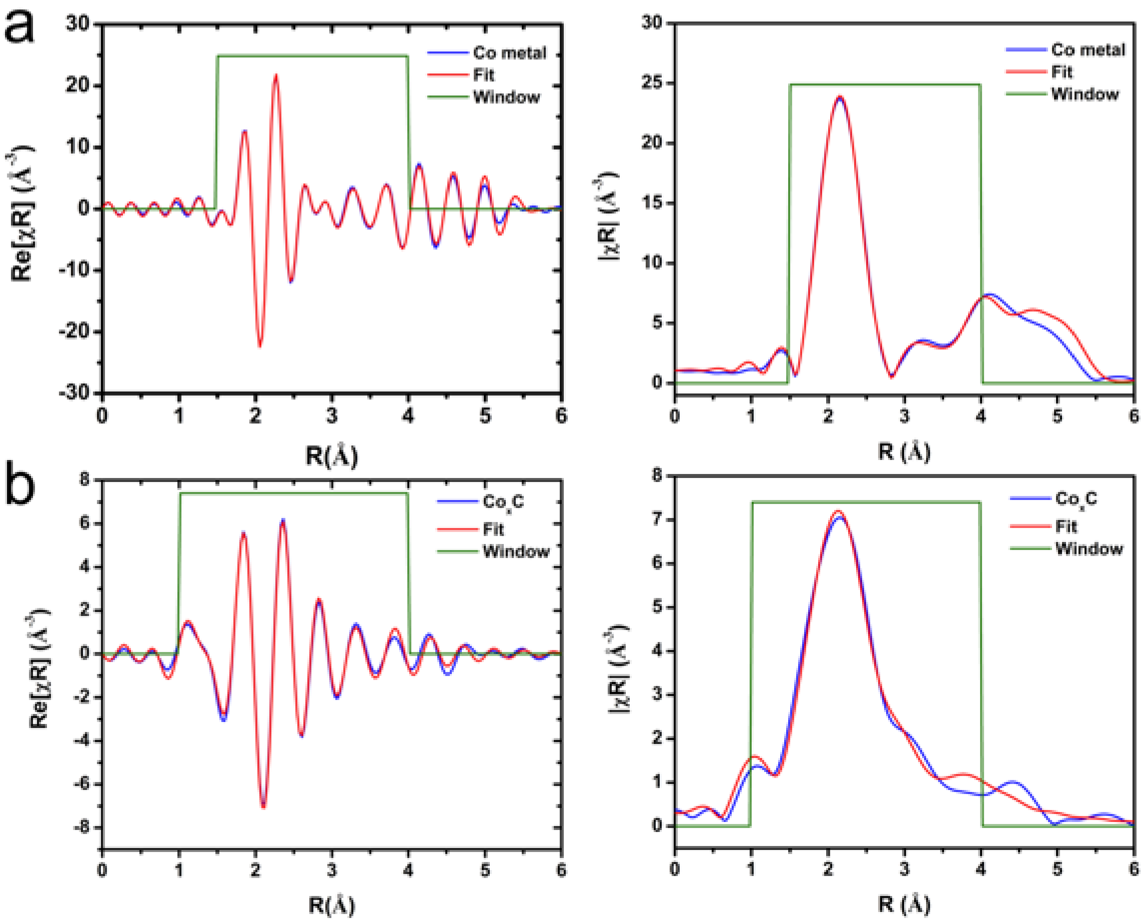

Figure S7. Left: k^3-weighted real FT vs. *R* experimental EXAFS results and theoretical fit with Artemis at the Co K-edge for the final reaction products; and right: k^3-weighted Fourier transform experimental results and theoretical fit up to and including the third Co-Co (a) and Co-C (b) coordination shell.

The crystal structures of HCP and FCC Co metal (space group : P63/mmc and Fm-3m, respectively) and Co_2C and Co_3C (space group : Pnnm and Pnma, respectively) were used as input models for the fitting procedure. The Co-Co and Co-C distances correspond well with the distances reported in the reference crystal structures. As can be seen in Tables S4, good fits have been obtained with low R-factors and σ^2.

Table S4. EXAFS best fitting parameters; Co *K*-edge data*

RXN	**Bond Lengths**		**R-factor**	**σ^2**
	Co-Co (Å)	Co-C (Å)		(Å^2)
Co-Metal	2.942 ± 0.007	-	0.0007	0.714
Co-Carbide	2.491 ± 0.013	1.766 ± 0.002	0.001	0.729

* Ranges used : $\Delta k = 2 - 8$ Å^{-1} and $\Delta R = 1- 4$ Å

References

1 *International Journal of Spectroscopy*, 2011, **2011**.
2 F. Tuinstra and J. L. Koenig, *J Chem Phys*, 1970, **53**, 1126.
3 A. C. Ferrari and J. Robertson, *Physical Review B*, 2000, **61**, 14095-14107.
4 J. Robertson, *Mat Sci Eng R*, 2002, **37**, 129-281.
5 B. N. Papas and H. F. Schaefer, *J Chem Phys*, 2005, **123**.
6 R. Clerac, F. A. Cotton, K. R. Dunbar, T. B. Lu, C. A. Murillo and X. P. Wang, *Inorg Chem*, 2000, **39**, 3065-3070.
7 M. A. Watzky, E. E. Finney and R. G. Finke, *Journal of the American Chemical Society*, 2008, **130**, 11959-11969.
8 M. A. Watzky and R. G. Finke, *Journal of the American Chemical Society*, 1997, **119**, 10382-10400.